Proceedings of the 6th International Conference on the Application of Physical Modelling in Coastal and Port Engineering and Science (Coastlab16)

Ottawa, Canada, May 10-13, 2016

INVESTIGATION OF VOID FRACTIONS AND BUBBLE PLUME PROPERTIES UNDER BREAKING WAVES

LIAN TANG[1], ONYX W.H WAI[2], PENGZHI LIN[3]

1 Department of Civil and Environmental Engineering, The Hong Kong Polytechnic University, Hong Kong, tanglian.scu@163.com

2 Department of Civil and Environmental Engineering, The Hong Kong Polytechnic University, Hong Kong, onyx.wai@polyu.edu.hk

3 State Key Laboratory of Hydraulics and Mountain River Engineering, Sichuan University, Chengdu, China, cvelinpz@scu.edu.cn

ABSTRACT

Numerical investigation of turbulent flow field under breaking waves is still of great challenges, especially in the high intensity air bubble region, mainly due to the poor knowledge of bubble plume properties during wave breaking. In this study, the air entrainment model based on laboratory measured average air bubble size spectrum is incorporated into a two-dimensional numerical model (NEWFLUME) to investigate bubble plume evolutions under breaking waves in the surf zone. The model solves the Reynolds equations for turbulent flows and employs the volume-of-fluid (VOF) method to track free surfaces. The bubble entrainment process is simulated by using numerically computed instantaneous flow field and the experimentally determined model of bubble size spectrum. The simulated results of breaking wave height distribution, velocity profiles and the turbulent kinetic energy are verified by the experimental data. The void fractions and integral properties of bubble plume are examined and discussed.

KEYWORDS: breaking wave; bubble plume; void fractions

1 INTRODUCTION

In the surf zone, wave breaking generates high intensity of turbulence and entrains large volumes of air bubbles that can extend 0.5m or more below the surface and contribute significantly to the dynamics turbulent flow field (Deane and Stokes, 2002). The entrained air bubbles play an important role in wave energy dissipation (Rapp and Melville, 1990; Iafrati, 2011) and altering the turbulence and vortex field (Watanabe et al., 2005). To study these effects, a better understanding of the void fractions and bubble plume properties under breaking waves is important.

Several laboratory experiments studies on bubble plume under breaking waves in the surf zone have been conducted. Deane and Stokes (2002) measured the bubble size distribution under the laboratory-scale inside breaking waves. They found that the bubbles larger than about 1 mm have an initially bubble size density proportional to the bubble radius with power-law of -10/3 while the smaller bubbles with -3/2. Cox and Shin (2003) carried out laboratory studies on void fraction fluctuations in the region close to breaking wave front. They showed that the maximum ensemble-averaged void fractions were between 15 and 20%. Mori and Kakuno (2008) measured the void fraction and flow velocity under laboratory-scale breaking waves. They found that the void fraction shows linear dependence on the turbulence intensity. Blenkinsopp and Chaplin (2007) measured the time-dependent distribution of void fraction in laboratory. The results suggested that air entrainment and splash generation account for at least 6.5%~14% of the total energy dissipation, and the percentage increases with the intensity of the breaking wave. Lim et al. (2015) measured the velocities and void fraction under an unsteady plunging breaking in laboratory. They found that the void fraction shows linear growth and exponential decay rate.

Besides laboratory experiments, numerical modelling of bubble dynamics under breaking waves is still limited. Terrill et al. (2001) proposed a numerical model based on an advection-diffusion equation to describe populations in the surf zone without considering bubble entrainment processes. Moraga et al. (2008) developed a sub-grid model to determine the bubble source due to air entrainment under breaking waves. Shi et al. (2010) presented a 2-D model based on mixture theory. In their model, they related the air entrainment to turbulence production at the air-water interface. Ma et al. (2011) proposed an air entrainment model based on the assumption that the total energy required for bubble formation is linearly proportional to the turbulence dissipation rate ε , and then incorporated it in to a VOF model TRUCHAS (Rider and Kothe, 1998) to investigate

the bubble plume dynamics under breaking waves. Their model could predict the void fractions and bubble plume evolution well under spilling breaking wave but showed overestimation of the stream wise velocities above the still water level.

In this study, the experimentally based air entrainment model developed by Ma et al. (2011) is incorporated into the model NEWFLUME, which is developed by Lin and Xu (2006) for general turbulent surface flows simulations, to investigate the void fractions and bubble plume characteristics under breaking waves in the surf zone. The spilling regular wave run-up a 1/35 slope is simulated by the present model and the numerical results are verified by the measurement data of Cox and Shin (2003).

2 MODEL DESCRIPTION

In the present work, we consider the air-water mixture as a mixture phase and solve the mixture equations derived by Buscaglia et al (2002) for turbulent flow field, but add the additional shear stress term in the momentum equation to represent the momentum dissipation which caused by bubble-liquid interactions. The governing equations are given as:

$$\frac{\partial u_i}{\partial x_i} = 0 \tag{1}$$

$$\frac{\partial u_i}{\partial t} + u_j \frac{\partial u_i}{\partial x_j} = -\frac{1}{\rho_0}\frac{\partial p}{\partial x_i} + \frac{1}{\rho_0}\frac{\partial \left(\tau_{ij} + T_{Dij}\right)}{\partial x_j} + \frac{\rho}{\rho_0} g_i \tag{2}$$

where u_i is the mixture phase velocity of *i*-th component, $i = 1,\ 2$, t is the time, ρ is the mixture density and p is mixture phase pressure respectively. ρ_0 is the reference density for incompressible liquid phase, τ_{ij} is the Reynolds shear stress, T_{Dij} is the additional shear stress, g_i is the *i*-th component of the gravitational acceleration.

The mixture density is calculated by

$$\rho = \rho_a \alpha_a + \rho_w \left(1 - \alpha_a\right) \tag{3}$$

where ρ_a is the air density and ρ_w is the water density, α_a is the void fraction of the air bubbles. The turbulence closure is accomplished by the nonlinear $k-\varepsilon$ model (Lin and Liu, 1998a), the equations are given by:

$$\frac{\partial k}{\partial t} + u_j \frac{\partial k}{\partial x_j} = \frac{\partial}{\partial x_j}\left[\left(\frac{\nu_t}{\sigma_k} + \nu\right)\frac{\partial k}{\partial x_j}\right] - \left\langle u_i' u_j' \right\rangle \frac{\partial u_i}{\partial x_j} - \varepsilon \tag{4}$$

$$\frac{\partial \varepsilon}{\partial t} + u_j \frac{\partial \varepsilon}{\partial x_j} = \frac{\partial}{\partial x_j}\left[\left(\frac{\nu_t}{\sigma_\varepsilon} + \nu\right)\frac{\partial \varepsilon}{\partial x_j}\right] + C_{1\varepsilon}\frac{\varepsilon}{k} 2\nu_t \sigma_{ij} \frac{\partial u_i}{\partial x_j} - C_{2\varepsilon}\frac{\varepsilon^2}{k} \tag{5}$$

where *k* is turbulent kinetic energy and ε is the turbulence dissipation rate, ν is the kinematic molecular viscosity and ν_t is the eddy viscosity. C_d,σ_k, σ_ε, $C_{1\varepsilon}$ and $C_{2\varepsilon}$ are empirical coefficients (Rodi, 1980)

$$C_d = 0.09,\ \sigma_k = 1.0,\ \sigma_\varepsilon = 1.0,\ C_{1\varepsilon} = 1.44,\ C_{2\varepsilon} = 1.92 \tag{6}$$

The bubble plume population is calculated by solving the bubble number density equation, which is given by

$$\frac{\partial N_{b,n}}{\partial t} + \frac{\partial}{\partial x_j}\left(N_{b,n} u_{b,n}\right) = \frac{\partial}{\partial x_j}\left(\left(\frac{\nu_t}{\sigma_b} + \nu\right)\frac{\partial N_{b,n}}{\partial x_j}\right) + E_{b,n} \tag{7}$$

The void fraction can be calculated by

$$\alpha_a = \sum_{n=1}^{N} \frac{4}{3}\pi r_{b,n}^3 N_{b,n} \tag{8}$$

where $N_{b,n}$ is the bubble spectrum for the *n*-th bubble group, N is the total bubble group number, σ_b is the Schmidt number of gas, with $\sigma_b = 1.0$ (Carrica et al., 1998). $u_{b,n}$ is the bubble velocity for the *n*-th bubble group which with characteristic radius $r_{b,n}$, $E_{b,n}$ accounts for the bubble entrainment source from the free surface. The bubble velocity is calculated by

$$u_{b,n} = u_m + u_{r,n} \tag{9}$$

in which $u_{r,n}$ is the bubble rise velocity for the *n*-th bubble group, which is related to the bubble diameter $d_{b,n}$:

$$u_{r,n}=\begin{cases}\dfrac{2}{9}\dfrac{d_{b,n}^2 g}{\nu}\left(1-\dfrac{\rho_a}{\rho_w}\right) & d_{b,n}<0.068mm \quad (Falvery,\ 1980)\\ \dfrac{1}{18}\dfrac{d_{b,n}^2 g}{\nu}\left(1-\dfrac{\rho_a}{\rho_w}\right) & 0.068mm<d_{b,n}<0.8mm \quad (Comolet,\ 1979)\\ \sqrt{0.52gd_{b,n}+2.14\dfrac{\sigma_t}{\rho_w d_{b,n}}} & 0.8mm<d_{b,n}<10.0mm \quad (Comolet,\ 1979)\\ u_{ar}=\sqrt{gd_{b,n}} & d_{b,n}>10.0mm \quad (Falvery,\ 1980)\end{cases} \tag{10}$$

The bubble entrainment source $E_{b,n}$ is calculated by the formulation developed by Ma et al. (2011), which related the bubble entrainment with turbulence dissipation rate ε :

$$E_{b,n}=\frac{c_b}{4\pi}\left(\frac{\sigma}{\rho_l}\right)^{-1}(1-\alpha_\alpha)\frac{f\left(r_{b,n}\right)\Delta r_{b,n}}{\sum_{i=1}^{N} r_{b,n}{}^2 f\left(r_{b,n}\right)\Delta r_{b,n}}\varepsilon \tag{11}$$

where c_b is bubble entrainment coefficient, σ is surface tension, $\Delta r_{b,n}$ is the width of each bubble group and $f\left(r_{b,n}\right)$ is the bubble size spectrum, which is determined by experiment measured data of Deane and Stokes (2002). For bubbles larger than 1 mm, turbulent fragmentation determines bubble size distribution, resulting in an initially bubble density proportional to the bubble radius to the power of -10/3. Smaller bubbles are created by jet and drop impact on the wave face, with a -3/2 power-law scaling, which gives the bubble size spectrum as:

$$f\left(r_{b,n}\right)\propto\begin{cases} r_{b,n}{}^{-\frac{10}{3}}, & when\ \ r_{b,n}\le 1.0mm\\ r_{b,n}{}^{-\frac{3}{2}}, & when\ \ r_{b,n}>1.0mm\end{cases} \tag{12}$$

3 RESULTS AND DISCUSSIONS

A spilling breaking wave run-up on a 1/35 slope (Cox and Shin, 2003) is simulated by the presented model. The simulation setup is shown in Figure 1. The still water depth in the wave flume is h=0.51m, the wave train has a wave height H=0.11m with wave period T=2.0s. The measured breaking point is located at x_b=18.07m. Three measurement cross-sections are located at (a): x=18.81m, (b): x=18.94m and (c): x=19.17m respectively.

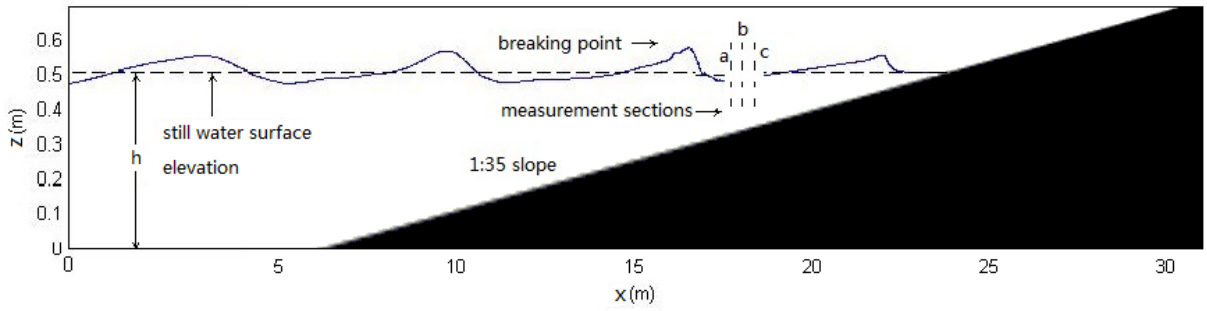

Figure.1 Sketch of the experiment setup and the computation domain.

In the numerical simulations, the computational domain is 31m long by 0.7m high, with the sloping beach toe 6.0m from the inlet boundary. The computational domain is discretized into a 1550×80 grids system with uniform grid $\Delta x=0.02m$ in the x direction, and non-uniform grid in the z direction with the minimum grid $\Delta z=0.006m$ near the free surface. The time step is automatically adjusted during the computation to satisfy the computation stability and to save the computation time.

3.1 Comparison of experimental data and numerical results

In this section, comparisons between the experimental data and numerical results are presented for the wave height, mean stream wise velocities and turbulence kinetic intensity. Figure 2 shows the comparison of wave height distribution, the simulated wave heights are in good agreement with the experimental data, although the predicted maximum wave height is a little smaller than measurement. Figure 3 shows the comparisons of mean velocities at three vertical cross-sections in the surf zone. At each location, comparisons are made at four different elevations z=0.5cm, -0.5cm, -1.5cm, -4.5cm from the still

water level. Though the simulated mean velocities are larger than the measurement in the lower region z=-4.5cm, the overall agreement between the numerical results and experimental data is acceptable, especially the maximum velocities above the still water level, which show good agreement with the measured data.

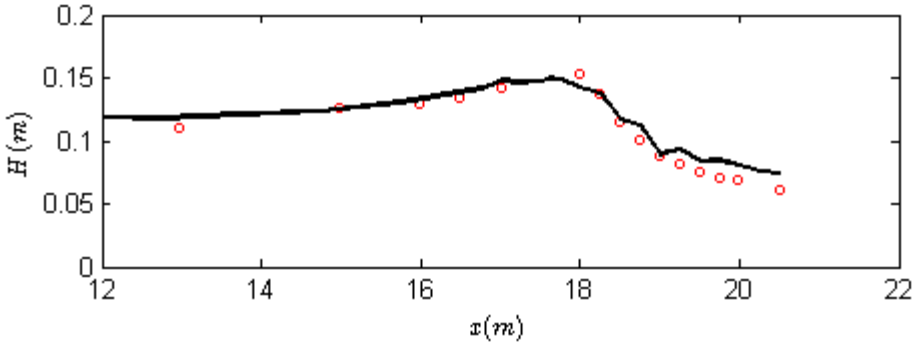

Figure.2 Comparisons of measured (dot) and simulated (solid line) wave heights along the flume.

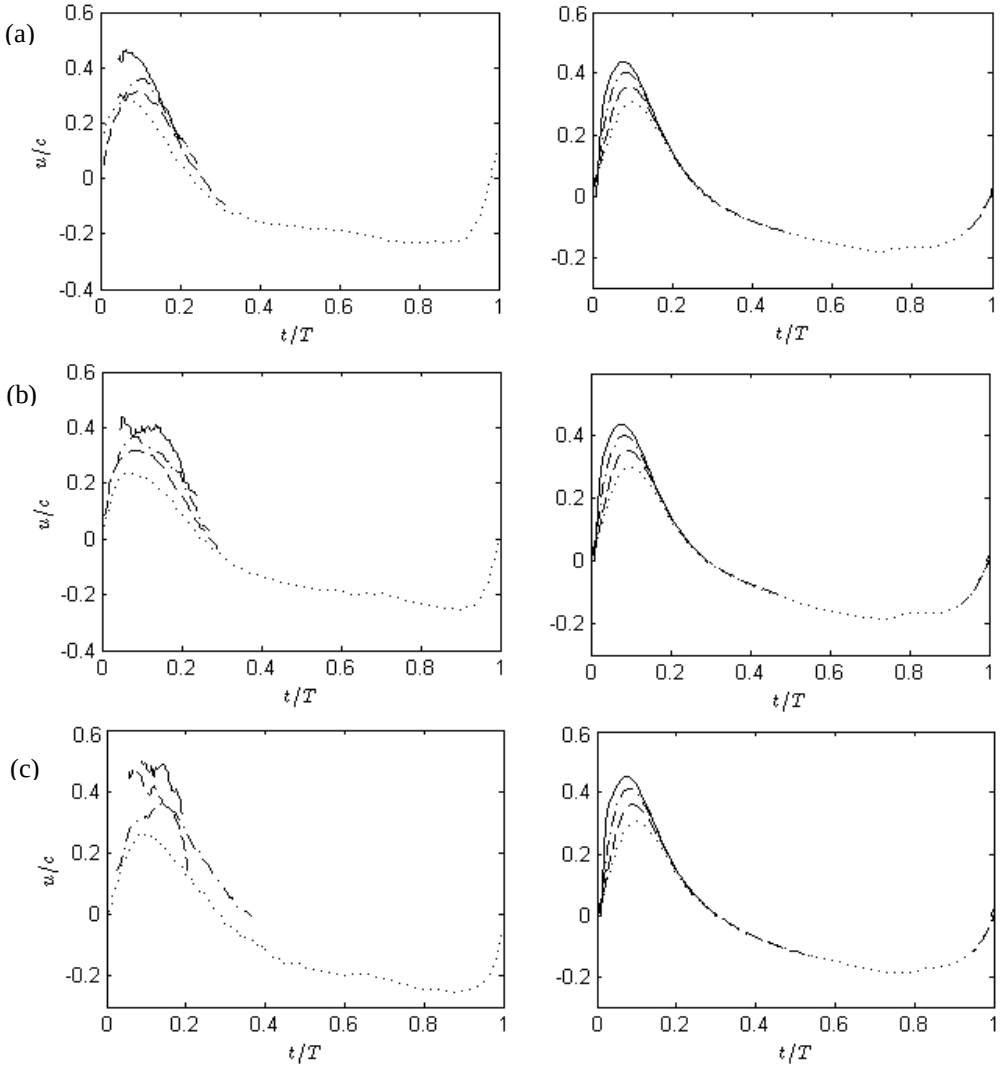

Figure.3. Comparisons of horizontal mean velocities between experimental data (left panels) and numerical results (right panels) at sections (a) *x*=18.81m, (b) *x*=18.94m and (c) *x*=19.17m across the water depth z=0.5cm (—), z=-0.5cm (-.-.), z=-1.5cm (---), z=-4.5cm (…).

Due to lack of measured turbulence kinetic intensity, the simulated turbulence intensity is compared with measured

horizontal velocity variance, which is shown in Figure 4. The simulated turbulence kinetic intensity shows multiple relation with the average value of the horizontal velocity variance. Besides, the decay trends between the turbulence intensity and the horizontal velocity variance are consistent. The comparisons with the measured data indicate that the present model is capable of simulating the turbulent flow field in the aeration region under breaking waves.

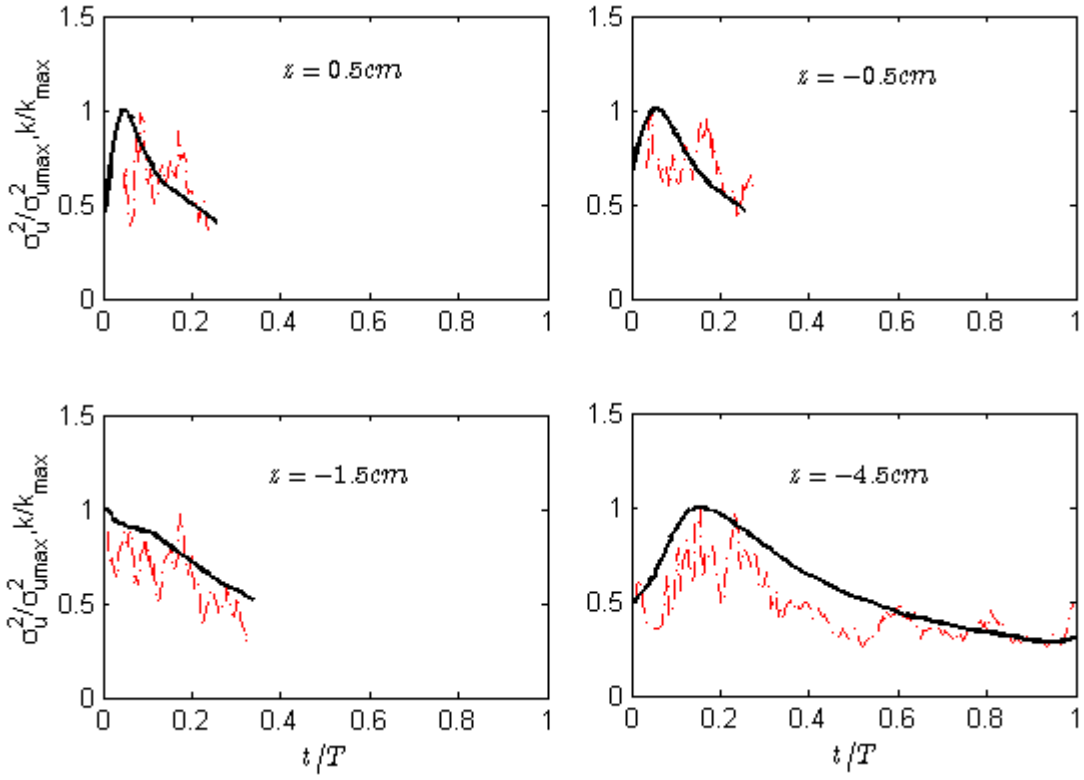

Figure.4. Comparisons of measured horizontal velocity variance and simulated turbulence kinetic intensity (solid line) at section b (x=18.94m) at different vertical locations.

3.2 Integral properties of bubble plume under breaking waves

The capability of the proposed model for predicting turbulent flow field under breaking waves has been tested and verified. In this following, the model is applied to investigate the integral properties of bubble plume. The characteristics of bubble plume can be described by the total volume of air entrained V, variation of the bubble plume area A and the potential energy of the entrained bubble plume E. They can be estimated by

$$V = \int_A \alpha_\alpha' dA \tag{13}$$

$$E = \int_A \alpha_\alpha' \overline{z}\, dA \tag{14}$$

where α_α' is void fractions with boundaries of 3% and 97% , $\overline{z}$ is the instantaneous vertical distance from grid center to the free surface. The integration region is conducted in $17.0m < x < 21.0m$ and $0.38m < z < 0.66m$, which covers the whole bubble plume evolutions area. The grids in this area with void fraction α_α' between 3% and 97% will be recorded to calculate bubble plume area A and to integrate the above equations.

Comparisons of void fraction distributions at three vertical cross-sections are shown in Figure 5. The overall numerical results agree well with the measured data with the predicted void fraction with maximum value 25% is about 10% higher than the measured data at section (a), z=1.5cm; though the model shows underestimation of the void fraction at section (b), z=2.5cm and section (c), z=1.5cm. It can be found that the void fraction decreased rapidly and changed to nearly zero within $0.1T$ after wave breaks, which indicates that almost all the entrained bubbles degassed in $0.1T$. This finding is consistent with the experimental results of Lamarre and Melville (1991), which showed that the degassing rate after wave breaking was very quickly, and less than 5% of the initial entrained bubbles remained in the water column one period after breaking.

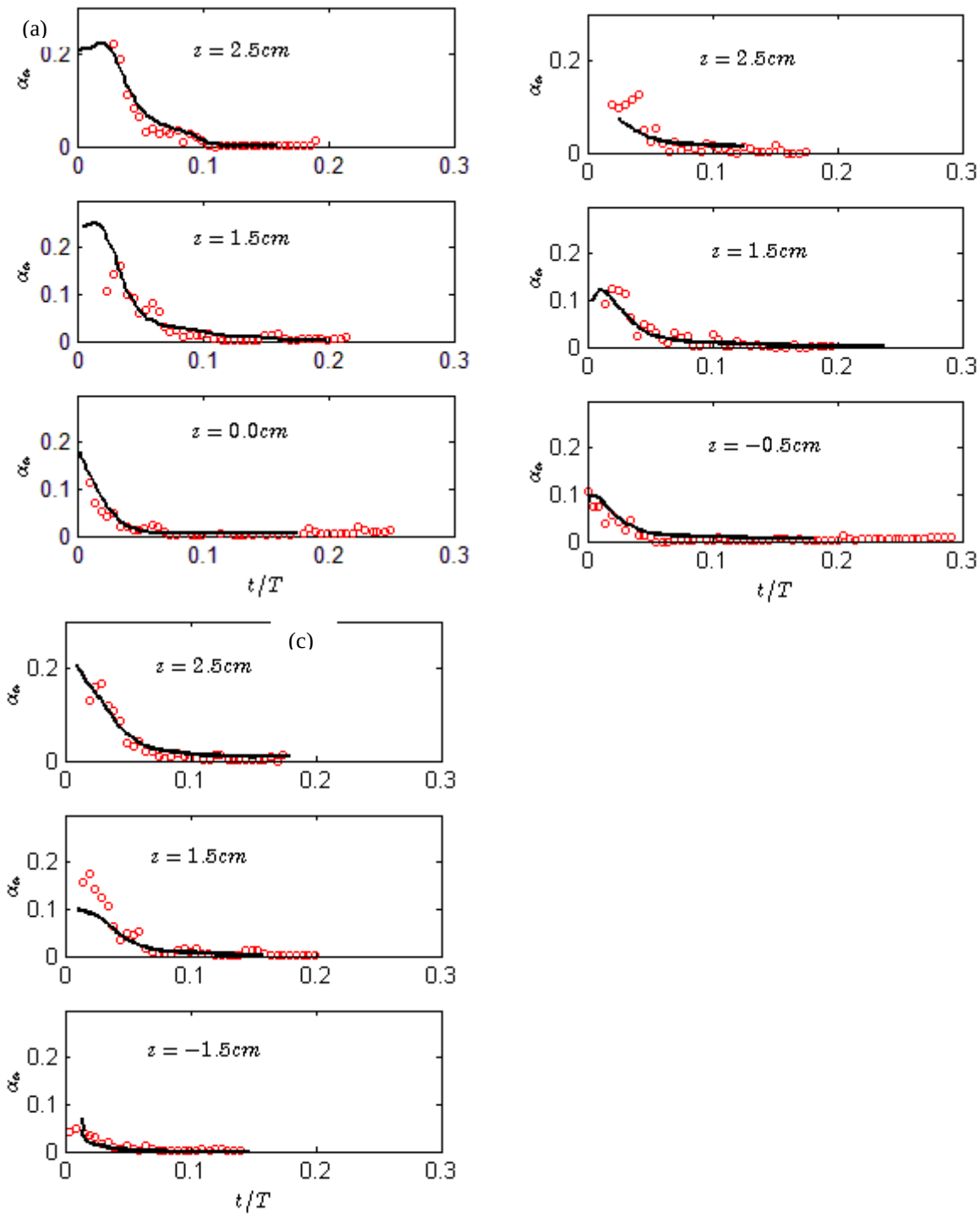

Figure.5. Comparisons of measured (dot) and simulated (solid line) void fractions at different vertical elevations at cross-sections (a) x=18.81m, (b) x=18.94m and (c) x=19.17m.

Figure 6 shows the evolutions of bubble plume volume and bubble plume area, which are normalized by the peak value in a wave cycle V_{max} and A_{max} , respectively. The volume increase rapidly and reaches the peak value at 0.22T after wave breaks. Then, the volume decays similarly in an exponential way as the bubble plume degasses. A second peak is observed around 0.35T, which could be connected with the air entrainment induced by the bore impingement on the slope. Compared with the volume, the bubble plume area shows a mild decay trend, and is in no hurry to decay after reaching the maximum value, but maintain a constant value for about half a wave period. This is mainly contributed to the diffusion processes of bubbles in the water, especially the small bubbles, which have smaller rise velocities (buoyancy forces) and can stay for longer time in the water. This also indicates that the void fractions under breaking waves are dominated by the entrained larger bubbles. The potential energy of the bubble plume, which also can be described as the energy that are required to maintain the entrained

bubbles in the water is shown in Figure 7. Similar to the bubble plume volume, two peaks are observed for the bubble plume potential energy. The decay trend of potential energy is consistent with the decay of bubble plume volume, which indicates that the air entrainment processes is closely related to the energy dissipation during wave breaking.

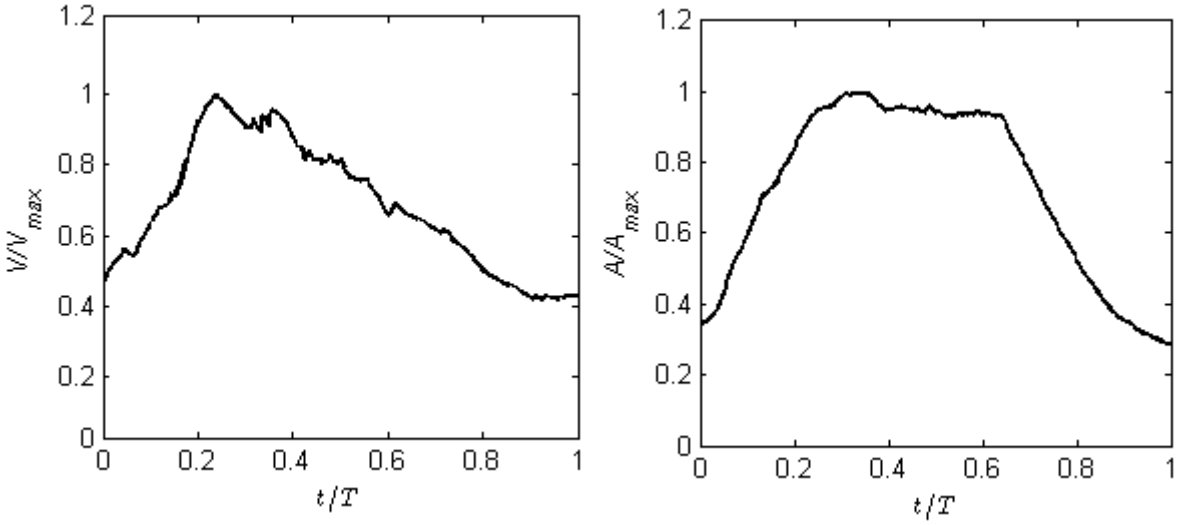

Figure.6. Volume per unit width of bubble plume, $V/V_{\max}$, and the bubble plume area $A/A_{\max}$.

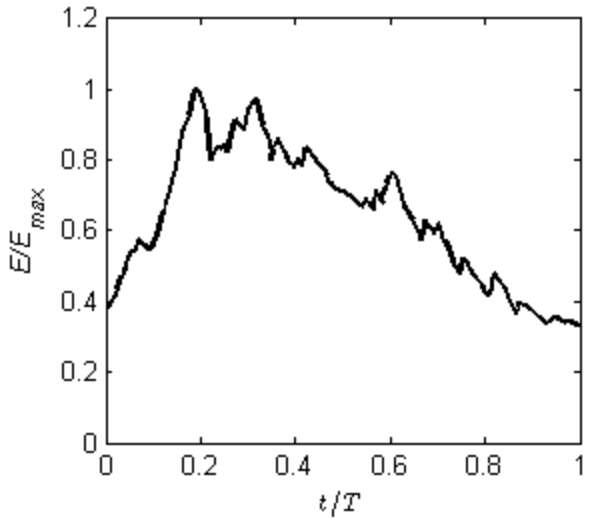

Figure.7. Potential energy of the entrained bubble plume $E/E_{\max}$.

4 CONCLUSIONS

In this study, the air entrainment model based on experimentally determined initial bubble size spectrum distribution under the laboratory-scale breaking waves is incorporated into the numerical model NEWFLUME to investigate the breaking waves in the surf zone. The bubble entrainment process is simulated by using numerically computed instantaneous flow field and the laboratory based bubble size spectrum. The reliability of the model is validated in terms of wave height evolution, mean velocity, and turbulence intensity. Then, the model is applied to studies the void fractions and bubble plumes properties. The void fraction distributions with maximum value up to 25% in the region close to the breaking point are well captured by the model, though it shows slightly overestimation and underestimation at some locations, the overall comparisons are good. The evolutions of bubble plume volume and potential energy show similar increase and decay trend, they reach the maximum value around $0.2T$ rapidly and decay similarly in an exponential way as the degassing of the entrained bubbles. The bubble plume area maintains the maximum value as long as half a wave cycle, and shows mild decay rate due to the small bubbles diffusion effects.

ACKNOWLEDGEMENT

The study was supported, in part, by the Hong Kong Research Grants Council (Grant No: PolyU 5273/12E),National Natural Science Foundation of China (Grant No: 51279120).

REFERENCES

Buscaglia, G. C., Bombardelli, F. A., García, M. H., 2002. Numerical modeling of large-scale bubble plumes accounting for mass transfer effects. *International journal of multiphase flow*, 28(11), 1763-1785.

Blenkinsopp, C. E., and J. R. Chaplin., 2007. Void fraction measurements in breaking waves, *Proc. R. Soc*. A, 463, 3151-3170.

Carrica, P., Bonetto, F., Drew, D., Lahey, R., 1998. The interaction of background ocean air bubbles with a surface ship. *International journal for numerical methods in fluids*, 28(4), 571-600.

Cox, D. T., Shin, S., 2003. Laboratory measurements of void fraction and turbulence in the bore region of surf zone waves. *J. engineering mechanics*, 129(10), 1197-1205.

Deane, G. B., Stokes, M. D., 2002. Scale dependence of bubble creation mechanisms in breaking waves. *Nature*, 418(6900), 839-844.

Comolet, R. (1979). Terminal velocity of a gas bubble in a liquid very low viscosity. *Journal of mechanical application*, *3*(2), 145-171.

Falvey, H. T. (1980). Air-water flow in hydraulic structures. *NASA STI/Recon Technical Report N*, *81*, 26429.

Iafrati, A., 2011. Energy dissipation mechanisms in wave breaking processes: Spilling and highly aerated plunging breaking events. *Journal of Geophysical Research: Oceans (1978–2012)*, *116*(C7).

Lamarre, E., Melville, W. (1991). Air entrainment and dissipation in breaking waves. *Nature*, *351*(6326), 469-472.

Lim,H.-J., K.-A. Chang, Z.-C.. Huang., B. Na, 2015. Experiment study in plunging breaking waves in deep water, *J. Geophys.Res. Oceans*, 120, 2007-2049.

Lin, P., Liu, P. L.-F.,1998a. A numerical study of breaking waves in the surf zone. *Journal of Fluid Mechanics*, 359, 239-264.

Lin, P., Xu, W., 2006. NEWFLUME: a numerical water flume for two-dimensional turbulent free surface flows. *J. Hydraulic Res*, 44(1), 79-93.

Ma, G., Shi, F., Kirby, J.T., 2011. A polydisperse two-fluid model for surf zone bubble simulation. *J. Geophys Res*: *Oceans*, (1978-2012),116(C5), doi:10.1029/2010JC006667.

Moraga, F. J., P. M. Carrica, D. A. Drew, and R. T. Lahey Jr., 2008. A sub-grid air entrainment model for breaking bow waves and naval surface ships, *Comput. Fluids*, 37, 281-298.

Mori, N., T. Suzuki, and S. Kakuno., 2007. Experimental study of air bubbles and turbulence characteristics in the surf zone, *J. Geophys. Res*., 112, C05014, doi:10.1029/2006JC003647.

Rapp, R., Melville, W., 1990. Laboratory measurements of deep-water breaking waves. *Philosophical Transactions of the Royal Society of London. Series A, Mathematical and Physical Sciences*, *331*(1622), 735-800.

Rider W.J., Kothe D.B., 1998. Reconstructing volume tracking, *J. Comput. Phys*., 141, 112-152.

Rodi., 1980. Turbulence Models and Their Application in Hydraulics. *International Association for Hydraulic Research Publication*, 29-30.

Terrill, E. J., W. K. Melville, and D. Stramski., 2001. Bubble entrainment by breaking waves and their influence on optical scattering in the upper ocean, *J. Geophys. Res*., 106, 16,815–16,823.